Title

Epidermal Cells Are the Primary Phagocytes in the Fragmentation and Clearance of Degenerating Dendrites in Drosophila

Journal

Neuron, 81(3)

ISSN

0896-6273

Authors

Han, Chun
Song, Yuanquan
Xiao, Hui
et al.

Publication Date

2014-02-01

DOI

10.1016/j.neuron.2013.11.021

Peer reviewed

Published in final edited form as:
Neuron. 2014 February 5; 81(3): 544–560. doi:10.1016/j.neuron.2013.11.021.

Epidermal cells are the primary phagocytes in the fragmentation and clearance of degenerating dendrites in *Drosophila*

Chun Han[#1], **Yuanquan Song**[#1], **Hui Xiao**[2], **Denan Wang**[1], **Nathalie C. Franc**[2], **Lily Yeh Jan**[1], and **Yuh-Nung Jan**[1,*]

[1]Howard Hughes Medical Institute, Departments of Physiology, Biochemistry and Biophysics, University of California, San Francisco, Rock Hall, 1550 4th Street, San Francisco, CA 94158, USA

[2]Department of Immunology & Microbial Sciences, The Scripps Research Institute, 10550 N. Torrey Pines Rd, La Jolla, CA92037, USA

[#] These authors contributed equally to this work.

SUMMARY

During developmental remodeling, neurites destined for pruning often degenerate on-site. Physical injury also induces degeneration of neurites distal to the injury site. Prompt clearance of degenerating neurites is important for maintaining tissue homeostasis and preventing inflammatory responses. Here we show that in both dendrite pruning and dendrite injury of *Drosophila* sensory neurons, epidermal cells rather than hemocytes are the primary phagocytes in clearing degenerating dendrites. Epidermal cells act via Draper-mediated recognition to facilitate dendrite degeneration and to engulf and degrade degenerating dendrites. Using multiple dendritic membrane markers to trace phagocytosis, we show that two members of the CD36 family, *croquemort* (*crq*) and *debris buster* (*dsb*), act at distinct stages of phagosome maturation for dendrite clearance. Our finding reveals the physiological importance of coordination between neurons and their surrounding epidermis, for both dendrite fragmentation and clearance.

INTRODUCTION

During development, many neurons remodel their dendritic arbors and axon projections to establish functional circuits, often involving pruning of dendrites and axons (Luo and O'Leary, 2005; Williams and Truman, 2005) undergoing degeneration similar to that induced by physical injury or pathological conditions (Saxena and Caroni, 2007; Tao and Rolls, 2011). In both pruning and pathological degeneration, neuronal debris needs to be swiftly removed. Efficient clearance of neuronal debris not only facilitates neurite regrowth

[*]Correspondence: yuhnung.jan@ucsf.edu.

(Hall, 2005) but also prevents inflammation, which could cause or exacerbate neurodegeneration (Frank-Cannon et al., 2009).

Similar to apoptotic cells, degenerating neuronal processes are cleared via engulfment by phagocytes. Besides professional phagocytes such as macrophages, several other cell types can play the role of phagocytes in organisms ranging from worms to mammals (Etchegaray et al., 2012; Inoue et al., 2000; Ishizaki et al., 1993; Li and Baker, 2007; Wood et al., 2000; Zhou et al., 2001). Phagocytosis of degenerating axons is mainly carried out by glia in the central nervous system (CNS) (Aldskogius and Kozlova, 1998; Awasaki and Ito, 2004; MacDonald et al., 2006; Watts et al., 2004) and sometimes assisted by macrophages in the peripheral nervous system (PNS) (Hall, 2005). The elimination of degenerating dendrites in the CNS is most likely also executed by glia (Marin-Teva et al., 2004). It is unclear how degenerating peripheral neurites, such as insect sensory dendrites and vertebrate sensory axons innervating the skin, are cleared. Although macrophage-like hemocytes have been reported to engulf dendrite debris during pruning of *Drosophila* sensory neuronal dendrites (Williams and Truman, 2005), it is unknown whether hemocytes are primarily responsible for clearing the massively pruned dendrites during metamorphosis or the degenerating dendrites resulting from injury.

Studies of glia-mediated clearance of degenerating axons resulting from pruning or injury in *Drosophila* have revealed the important role of the engulfment receptor Draper (Drpr), used by phagocytes in engulfing cell corpse, axon debris, and destabilized synaptic boutons (Awasaki et al., 2006; Cuttell et al., 2008; Etchegaray et al., 2012; Fuentes-Medel et al., 2009; MacDonald et al., 2006). The CD36 family is also implicated in phagocytosis (Silverstein and Febbraio, 2009; Stuart and Ezekowitz, 2008). In mammals, CD36 acts together with thrombospondin and integrins for engulfment of apoptotic cells *in vitro* (Savill et al., 1992). A *Drosophila* CD36 family member, Croquemort (Crq), is required for efficient clearance of apoptotic cells by embryonic macrophages (Franc et al., 1999). The *Drosophila* genome encodes fourteen CD36 family members (Nichols and Vogt, 2008). Crq and Peste (Pes) have been implicated in phagocytosis of bacterial pathogens (Philips et al., 2005; Stuart et al., 2005), but the roles of the CD36 family in the clearance of apoptotic cells or cellular debris have not been systematically explored.

Once engulfed by phagocytes, neuronal debris undergoes degradation through the endosome-lysosome pathway (Doherty et al., 2009; Song et al., 2008; Watts et al., 2004), likely resembling the phagocytosis of apoptotic cells by professional phagocytes. Engulfment of cell corpses produces nascent phagosomes, which undergo maturation to sequentially transform into early phagosomes, late phagosomes, and ultimately phagolysosomes (Botelho and Grinstein, 2011; Kinchen and Ravichandran, 2008; Zhou and Yu, 2008). Phagosome maturation is a highly coordinated process that involves membrane fission and fusion with endosomes and lysosomes under the control of vesicle-trafficking regulators such as Rab GTPases. During this process, phagosomes become increasingly acidified and hydrolase-rich, leading to degradation of internalized particles. Studies of phagosome maturation traditionally involve examining the engulfment of opsonized particles or microbes by isolated macrophages and cultured cells. Recent genetic studies and live imaging have examined the *in vivo* function of phagosome components in *C. elegans*

(Zhou and Yu, 2008). Notwithstanding the significant knowledge gleaned for the major steps of phagosome maturation, further development of markers that label discrete steps of phagosomal acidification and degradation will improve our understanding of this cellular process.

Drosophila dendritic arborization (da) neurons have emerged as a useful system for studying both developmentally regulated and injury-induced dendrite degeneration. The da neurons are multi-dendritic sensory neurons growing underneath the body wall. Dendritic arbors of da neurons degenerate during metamorphosis as a result of apoptosis or dendrite pruning (Kuo et al., 2005; Williams and Truman, 2005). Severing of larval da neuronal dendrites also triggers degeneration of distal dendrites (Song et al., 2012; Tao and Rolls, 2011). In this study, we explored the roles of different cell types in the clearance of degenerating dendrites, and found that the adjacent epidermal cells are primarily responsible for the removal of dendrite debris. We used a series of dendritic markers to trace the maturation of phagosomes containing engulfed dendrite debris *in vivo* and delineated the sequential actions of several genes in the phagocytosis pathway. We found that loss of function of *crq* caused extensive phagosome fusion accompanied with inefficient degradation but did not affect engulfment of dendrite debris. We further identified another CD36 family member that we named Debris buster (Dsb) with essential roles at the late stage of phagosome maturation. Moreover, efficient dendrite fragmentation requires coordination between dendrites and the adjacent phagocytic epidermal cells. Together, these results reveal that epidermal cells are active participants in the destruction of degenerating dendrites in both dendrite remodeling and following injury, and provide a genetic platform for uncovering the molecular mechanisms of engulfment and phagosome maturation.

RESULTS

Degenerating dendrites are primarily cleared by the epidermal epithelium rather than by macrophages

By using *ppk-CD4-tdGFP* that specifically and brightly labels all dendritic processes of class IV da neurons (Han et al., 2011), we monitored dendrite degeneration and the disappearance of dendrite debris *in vivo*, and chose to focus on the dorsal class IV da neuron ddaC for consistency. Soon after the larva enters the prepupal stage (puparium formation) (Figure 1A), ddaC initiates a series of dendrite destruction programs including shedding of membrane vesicles called “shedosomes”, severing of proximal dendrites, thinning and beading of low order branches, and dendrite fragmentation (Han et al., 2011; Kuo et al., 2005; Lee et al., 2009; Williams and Truman, 2005). By the end of prepupal stage at 12 hr after puparium formation (APF), all proximal dendrites had been severed and the majority of dendrites had degenerated and disappeared (Figure 1B). Dendrite degeneration and clearance was complete by 16 hr APF (Figure 1C). For the dendrite injury model, we severed proximal dendrites of ddaC near the soma (arrowhead in Figure 1D) in the larva at 72 hr after egg laying (AEL) with an infrared laser, which induces degeneration of all dendrites distal to the injury site (Song et al., 2012). The severed dendrites showed signs of degeneration, such as blebbing and fragmentation, at 3 hr after injury (AI) (Figure 1D) and

mostly broke down by 6 hr AI (Figure 1D'). By 12 hr AI, dendrite debris had been completely cleared (Figure 1D").

Which cell type is responsible for clearing disintegrated dendrites? *Drosophila* macrophages, or plasmatocytes, are professional phagocytes of the hemocyte lineage that clear apoptotic cells during development and engulf invading microorganisms as the major means of innate immunity (Braun et al., 1998; Tepass et al., 1994). Whereas plasmatocytes need to penetrate the extra cellular matrix to access dendrites (Han et al., 2012), they have been observed to engulf and carry pruned dendrites of da neurons (Williams and Truman, 2005). We reexamined the role of plasmatocytes by conducting time-lapse imaging of dendrite pruning with *ppk-CD4-tdGFP* to mark class IV da neurons and *pxn-Gal4 UAS-CD4-tdTom* to label plasmatocytes (Figure S1A). During metamorphosis, plasmatocytes extended membrane protrusions and migrated along the body wall, but rarely engulfed dendrite debris (Movie S1). We only observed 2 plasmatocytes engulfing dendrite membrane during the pruning of 23 neurons monitored with time-lapse imaging. Similar results were obtained with another hemocyte-specific driver hml^{Δ}*-Gal4* (data not shown). Moreover, genetic ablation of plasmatocytes via the expression of pro-apoptotic genes *reaper* (*rpr*) and *Wrinkled* (*W*) with *pxn-Gal4* (Figure S1B) did not affect the clearance of degenerating dendrites (Figures S1C' and S1D'), although some dendrites failed to fragment in a subset of segments by 18 hr APF (Figures S1C and S1D). In the dendrite injury model, plasmatocyte ablation appeared to delay dendrite fragmentation when examined at 5.5 hr AI (Figures S1E and S1F), but did not prevent degeneration or clearance of injured dendrites by 10 hr AI (Figures S1G and S1H). The effectiveness of plasmatocyte ablation was confirmed by the absence of intact plasmatocytes labeled by *pxn-Gal4 UAS-CD4-tdTom* (Figures S1B, S1D', S1F, and S1H). These data demonstrate that plasmatocytes are not required for the clearance of degenerating dendrites, although they appear to contribute to dendrite fragmentation.

Dendrites of larval da neurons grow along the basal surface of the epidermal epithelium (Han et al., 2012; Kim et al., 2012). In pupae with epidermal cells labeled by $Gal4^{5\text{-}56}$-driven tdTomato (tdTom), newly formed dendrite debris quickly dispersed into the epidermal layer before disappearing (Figure 1E). Similarly, debris derived from injured dendrites also entered the larval epidermal layer labeled by $Gal4^{A58}$ *UAS-tdTom* before disappearing (Figure 1F). These observations led us to propose and test the hypothesis that epidermal cells actually engulf and degrade dendrite debris (Figure 1G).

In *C. elegans*, dynamin is required for phagocytes to extend their membrane around cell corpses (so called "pseudopod extension") (Yu et al., 2006). While dendrite debris was efficiently removed in control *Drosophila* prepupae raised at 29°C (Figure 1H), inhibition of *Drosophila* dynamin Shibire (Shi) through over-expressing the temperature sensitive allele shi^{ts} specifically in epidermal cells prevented clearance of dendrite debris (Figure 1I); the remaining dendrite fragments maintained the dendrite branching patterns at the basal side of epidermal cells (bottom panel of Figure 1I). Similarly, debris of injured dendrites was completely cleared in control larvae raised at 29°C by 18 hr AI (Figure 1J), while epidermal expression of shi^{ts} potently blocked the spreading of debris into larval epidermal cells and its subsequent degradation (Figure 1K). Shi^{ts}-expressing animals showed normal speed of

dendrite clearance at the permissive temperature 18°C in both dendrite pruning (Figures S1I and S1J) and dendrite injury (Figures S1K and S1L). These results reveal that epidermal cells are the main phagocytes in clearing degenerating dendrites both during dendrite pruning and after dendrite injury.

Dendritic markers for analyzing the progression of phagocytosis of degenerating dendrites *in vivo*

The CD4-tdGFP marker allows us to trace degeneration and clearance of dendrites in live animals, but does not provide further information on how dendrite-derived phagosomes mature once GFP loses fluorescence or undergoes proteolysis. Unlike GFP, derivatives of the *Anthozoa* fluorescent protein DsRed, such as tdTom, are highly stable and resistant to degradation mediated by both proteasomes and lysosomes (Katayama et al., 2008; Verkhusha et al., 2003). In animals expressing *ppk-CD4-tdGFP* and *ppk-CD4-tdTom*, tdTom labeled a much broader pattern of dendrite debris than GFP during dendrite pruning (Figures 2A-2A”). In fact, the entire epidermal epithelium was occupied by small GFP-negative, tdTom+ particles by 12 hr APF (Figure S2A-S2A”). In later pupal stages (16-20 hr APF), while GFP signal was absent (Figure 2B), tdTom signal was gradually enriched in large, patchy structures in every epidermal cell (Figure 2B’), and persisted until new epidermal cells derived from histoblast nests eventually replaced larval epidermal cells (data not shown). Most of the small vesicles and large patchy structures coincided with the late phagosome/phagolysosome marker Rab7-GFP and the phagolysosome marker GFP-LAMP expressed by epidermal cells (Figures 2C-2D”), suggesting that they are phagolysosomes (Botelho and Grinstein, 2011; Pulipparacharuvil et al., 2005). Similarly, with larval dendrite injury, tdTom marked many more particles than GFP (Figures S2B-S2B”); tdTom signals eventually disappeared by 20 hr AI (Figure S2E’). The sustained labeling of phagosomes by the dendritic marker CD4-tdTom thus offers a unique advantage for analyzing late stages of phagosome maturation.

Immediately after completion of engulfment the nascent phagosomes undergo initial acidification, reducing the pH from neutral to below 6.5 (Botelho and Grinstein, 2011). We therefore fused ecliptic pHluorin to the extracellular side of CD4-tdTom to generate the membrane-associated pH sensor (MApHS) (Figure 2E) for monitoring pH changes. Ecliptic pHluorin (Miesenbock et al., 1998) is brightest at pH 7.5 under 475-nm excitation but gets dimmer as pH drops and loses fluorescence at pH below 6.0. Dendrite debris labeled by MApHS is expected to lose green fluorescence of pHluorin and retain red fluorescence of tdTom upon initial acidification of phagosomes (Figure 2F). Indeed, in areas where dendrite debris was continuously generated, pHluorin in *ppk-MApHS* only labeled a subset of tdTom + puncta in dendrite pruning (Figures 2G-2G”) and after dendrite injury (Figures S2C-2C”). Time-lapse imaging of dendrite pruning revealed that MApHS quickly lost pHluorin signals upon shedosome formation (Figures 2H-2H” and Movie S2) or dendrite fragmentation (Movie S3), suggesting that epidermal cells efficiently engulf disintegrated dendrites. The loss of pHluorin signals is due to quenching rather than degradation, as washing the samples with pH-neutral buffer after fixation restored green signals in many phagosomes (Figure S2D-S2D”).

Together, the dendritic markers CD4-tdGFP, CD4-tdTom, and MApHS constitute a tool kit for analyzing phagosome maturation during dendrite clearance by epidermal cells.

Testing dendritic markers in genetic dissection of dendrite clearance

Phagocytes clear cell corpses or cellular debris through several distinct stages. Besides dynamin in pseudopod extension, GTPases Rab5, Rab7, and lysosome-associated-membrane protein 1 (LAMP1) are key components of early phagosomes, late phagosomes, and phagolysosomes, respectively (Botelho and Grinstein, 2011). The functions of these molecules in phagocytosis have been studied in *C. elegans* and mammalian phagocytes (Huynh et al., 2007; Kinchen and Ravichandran, 2008; Zhou and Yu, 2008) but are largely uncharacterized in *Drosophila*. To test the utility of the three dendritic markers in analyzing various stages of dendrite clearance, we examined the loss-of-function phenotypes of *shi*, *Rab5*, *Rab7*, and *Lamp1* in epidermal cells using the GEEM (gene expression with an independent enhancer-driven cellular marker) strategy (Han et al., 2011) by expressing RNA interference (RNAi) constructs or dominant negative alleles.

We first analyzed dynamin by epidermis-specific expression of shi^{ts}. The pHluorin on MApHS-labeled dendrite debris in both pruning (Figures 3A-3B') and injury (Figures 3G-3H') models was completely quenched/degraded in control animals at 29°C (Figures 3A, 3G, and 3O) but retained signals in the same dendritic patterns as tdTom when shi^{ts} was expressed in epidermal cells (Figures 3B, 3B', 3H, 3H', and 3O), consistent with the role of dynamin in engulfment. In contrast, Shi^{ts} expression did not prevent the quenching of pHluorin at the permissive temperature 18°C (Figures S3A-S3D'). For both pruning (Figures 3C-3D') and injury (Figures 3I-3J'), *Rab5* knockdown blocked the quenching of pHluorin on MApHS-labeled dendrite debris (Figures 3D, 3D', 3J , 3J' and 3O). Unlike dynamin inhibition, persisting dendrite debris in *Rab5* knockdown was dispersed in the epidermal layer, consistent with the requirement of Rab5 in the initial acidification of phagosomes rather than engulfment. For Rab7 knockdown and subsequent RNAi experiments in pupae, we restricted the expression of RNAi constructs to the posterior half of every segment (En+) so that the anterior (En−) epidermal cells can serve as internal controls. Rab7 knockdown resulted in clearance defects in both dendrite pruning (pupae) and dendrite injury (larvae) as indicated by the lack of tdTom+ patchy phagolysosomes in the pupa (Figure 3E', En+ cells) and the presence of tdTom+ vesicles in the larva (Figures 3L and 3P). Although it did not interfere with pHluorin quenching (data not shown), loss of Rab7 partially blocked GFP degradation in dendrite pruning (pupa) (Figures 3E and 3P) but not after dendrite injury (larva) (Figures 3K and 3P). Knockdown of the only *Drosophila* LAMP gene, *Lamp1*, resulted in similar clearance defects in both dendrite pruning and dendrite injury: arrest of the maturation of tdTom-labeled phagosomes (Figures 3F', 3N, and 3P) without compromising GFP degradation (Figures 3F, 3M, and 3P). The effectiveness and specificity of *Rab5* and *Rab7 RNAi* constructs were confirmed by their ability to suppress the expression of corresponding GTPase-GFP fusion proteins, but not when the order is reversed (Figures S3E-S3I). We were not able to determine the effectiveness of *Lamp1 RNAi* due to the lack of Lamp1-GFP or a good antibody against Lamp1.

In the above experiments, *Rab7 RNAi*-expressing epidermal cells and wildtype (WT) epidermal cells showed differential abilities in degrading GFP (Figures 3K and 3E) and tdTom (Figures 3I' and 3C'), respectively, in dendrite injury (larval) and dendrite pruning (pupal) models. However, when we induced dendrite injury at the white pupa stage, the clearance of these injured dendrites in *Rab7 RNAi*-expressing epidermal cells (Figures S3J and S3J') and WT epidermal cells (Figure S3K) was similar to what was observed in dendrite pruning, suggesting that the capacity of the degradation machinery in pupal epidermal cells is attenuated compared to that of larval epidermal cells. Based on the roles of dynamin, Rab5, Rab7, and Lamp1 in phagocytosis and their loss-of-function phenotypes in pupae and larvae, we determined the stages of phagosome maturation which can be differentially labeled by the three dendritic markers in both pupal (open bars in Figure 3Q) and larval (solid bars in Figure 3Q) epidermal cells.

drpr is required for engulfment of dendrite debris by epidermal cells

With these tools, we sought to elucidate the molecular mechanisms of engulfment and phagosome maturation by identifying relevant genes, starting with genes implicated in phagocytosis in *Drosophila*. The engulfment receptor Drpr is involved in the removal of da dendrites during pruning (Williams et al., 2006). To test whether *drpr* is required by epidermal cells to clear dendrite debris, we examined epidermis-specific knockdown of *drpr* with the MApHS and CD4-tdGFP markers (Figures 4A-4B and 4G-4H) and confirmed the results in $drpr^{\Delta 5}$*/Df(3L)BSC181* mutants (Figures 4C-4D and 4I-4J, compared to WT in Figures S4A-S4B and Figures 4E-4F). Consistent with a role in engulfment, *drpr* knockdown blocked pHluorin quenching (Figures 4A, 4G, and 4K) and GFP degradation (Figures 4B, 4H, and 4M), with the dendrite debris retaining the pattern of intact dendrites in the larvae. $drpr^{\Delta 5}$*/Df(3L)BSC181* mutants showed clearance defects (Figures 4C-4D, 4G-4H, and 4K-4M) similar to those caused by *drpr* knockdown. Loss of *drpr* function produced weaker engulfment phenotypes in pupae than in larvae, as indicated by the acidification of many phagosomes (Figures 4E-4E") and the lower ratio of pHluorin+ areas over tdTom+ areas (Figure 4N) in pupae, raising the possibility that Drpr is not solely responsible for engulfment of dendrite debris for dendrite pruning. For glial clearance of apoptotic neurons in the developing CNS, *drpr* functions downstream of a bridging molecule *six-microns-under* (*simu*) after engulfment (Kurant et al., 2008). We found that, similar to WT controls (Figures S4C and S4E), the *simu* null mutant showed efficient clearance of CD4-tdGFP-labeled dendrite debris (Figures S4E and S4F). Our studies thus reveal that Drpr but not Simu is required for epidermal cells to engulf degenerating dendrites.

crq is required for phagosome maturation but not engulfment in dendrite clearance

The CD36 family member Crq is required for efficient phagocytosis of apoptotic cells in *Drosophila* embryos (Franc et al., 1999). To test whether *crq* is involved in dendrite clearance, we knocked down *crq* in the epidermis and found strong clearance defects as indicated by the absence of tdTom-labeled patchy phagolysosomes in pupal epidermal cells (Figures 5A' and 5B') and the presence of tdTom+ phagosomes in larval epidermal cells (Figures 5E' and 5I). pHluorin was detectable in very few vesicles in pupae (Figures 5A and 5I) but was mostly absent in larvae (Figures 5E and 5I). The ratios of pHluorin+ areas over

tdTom+ areas in *crq* knockdown were low compared to *drpr* knockdown (Figure 5J), indicative of normal engulfment. Comparison of GFP and tdTom signals revealed partial degradation of GFP in pupae (Figures 5B-5B" and 5K) but complete removal of GFP in larvae (Figures 5F and 5K). These data suggest that *crq* is not required for the engulfment of dendrite debris by epidermal cells but is necessary for phagosome maturation beyond the initial acidification.

The lack of engulfment defects in the *crq* knockdown is unexpected given earlier *in vitro* studies implicating Crq and human CD36 in the engulfment of apoptotic cells (Franc et al., 1996; Savill et al., 1992). Having obtained identical results with two *crq* RNAi lines that have no predicted off-targets, we next examined $crq^{KG01679}$, which harbors a P-element insertion in the promoter region of the *crq* locus, in trans-heterozygote with *crq* deficiency *Df(2L)al*, as well as a *crq* knockout null allele (crq^{ko}). We generated crq^{ko} to delete the entire coding region by using "end-out" gene targeting (Gong and Golic, 2003) (Figure S5E) and then validated it as a null mutant via genomic PCR (Figure S5F) and immunostaining (Figure S5G). Both $crq^{KG01679}$/*Df(2L)al* mutants (Figures S5A-S5D and 5I-5K) and crq^{ko} animals derived from homozygous mutant mothers (Figures 5C-5D, 5G-5H, and 5I-5K) showed the same clearance defects as *crq* knockdown, confirming a role for *crq* in phagosome maturation. Together, these results demonstrate that Crq plays a specific role in phagosome maturation but not in engulfment during dendrite clearance by epidermal cells.

Loss of *crq* leads to homotypic phagosome fusion during phagosome maturation

The arrested phagosomes in *crq* mutant epidermal cells appeared to be variable in size and brightness. Because the size difference of phagosomes may originate from engulfed dendrite fragments or phagosome fusion and fission, we examined the morphology of phagosomes in $crq^{KG01679}$/*Df(2L)al* epidermal cells by transmission electron microscopy (TEM). HRP-DsRed-GPI (Han et al., 2012) expressed on dendrites can be used to trace dendrite-derived phagosomes with DAB staining, as HRP remains active in degradative compartments (Dubois et al., 2001). Without post-embedding heavy metal staining and HRP expression, lysosomes/phagolysosomes in epidermal cells at 16 hr APF appear pale (Figure 6A), while phagolysosomes derived from HRP-labeled dendrite debris had dark staining (Figures 6B and 6C). Unlike phagolysosomes in WT epidermal cells that were characterized by heterogeneous contents such as vesicles, particles, and multi-layers of membrane (Figure 6C), the HRP-labeled phagosomes in $crq^{KG01679}$/*Df(2L)al* epidermal cells appeared more homogeneous in content (Figures 6D-6G). The variation in the extent of DAB labeling likely reflects the variable amounts of dendrite debris in these phagosomes. In contrast to the WT, $crq^{KG01679}$/*Df(2L)al* epidermal cells contained many large-size phagosomes (Figure 6H) that appeared to arise from phagosome fusion (Figures 6E-6G). As homotypic fusion rarely occurs among cell corpse-derived phagosomes (Kinchen and Ravichandran, 2008) or phagosomes in control epidermal cells, these observations implicate a direct or indirect role for *crq* in the prevention of homotypic phagosome fusion.

To characterize how Crq may regulate the dynamics of phagosome maturation, we conducted time-lapse imaging of dendrite pruning with the CD4-tdGFP marker. In the WT prepupa, newly formed phagosomes gradually lost GFP signals and became smaller (Figure

6I and Movie S4). In contrast, phagosomes in *crq* mutant cells often fused with one another (Figure 5J and Movie S5), leading to stronger GFP signals that persisted in these phagosomes. To determine the stage at which phagosome maturation is arrested, we incorporated the early phagosome marker GFP-2xFYVE (Wucherpfennig et al., 2003), which binds to PtdIns(3)P on the membrane of early phagosomes, and the late phagosome marker Rab7-GFP. We found that *crq* knockdown did not prevent recruitment of GFP-2xFYVE and Rab7-GFP to tdTom-labeled phagosomes during dendrite degeneration in prepupae (Figure S6A-S6A" and S6C-S6C") or larvae (Figure S6E-S6E" and S6G-S6G"). The dendrite-derived phagosomes were found to progress beyond the PtdIns(3)P+ early phagosome phase and Rab7+ late phagosome phase, as tdTom-labeled phagosomes no longer showed colocalization with GFP-2xFYVE or Rab7-GFP when examined at 18 hr APF in dendrite pruning (Figure S6B-S6B" and S6D-S6D") or 20 hr AI in dendrite injury (Figure S6F-S6F" and S6H-S6H"). Time-lapse imaging revealed that, in both WT (data not shown) and *crq*-knockdown epidermal cells (Figure 6K), Rab7-GFP was recruited to the periphery of phagosomes to form ring structures within 8-15 minutes of dendrite breakdown, and then released from the phagosomes after 30-60 minutes. The phagosomes became condensed upon dissociation with Rab7-GFP. In *crq*-knockdown (Figure 6K) but not WT cells, fusion and fission of tdTom-labeled phagosomes occurred frequently during and after the Rab7-GFP+ stage. Together, these data suggest that Crq is not necessary for phagosomes to progress through the Rab7+ stage but is required for the suppression of homotypic phagosome fusion and the degradation of phagosome contents.

drb is required for phagosome maturation during dendrite clearance

To identify new players in phagosome maturation, we conducted a small scale RNAi screen with selected candidate genes. We found that an uncharacterized CD36 family member, CG1887, is also involved in the clearance of degenerating dendrites. Knockdown of *CG1887* in the epidermis did not prevent initial phagosome acidification (data not shown) or block GFP degradation in pupae (Figures 7A and 7D) or larvae (Figures 7B and 7D), but it blocked formation of large patchy phagolysosomes in pupae (Figure 7A') and the degradation of tdTom in larvae (Figures 7C and 7D), suggesting that *CG1887* is required for the late phase of phagosome maturation. Based on the phenotype of incomplete clearance, we name *CG1887 debris buster* (*dsb*). The longest isoform of *dsb* transcripts encodes a double-span transmembrane protein of the CD36 family (Figure S7A). We were not able to examine the dendrite clearance phenotype in *dsb* mutants as the only available allele of *dsb*, dsb^{f07156}, which bears a PBac insertion in the coding region (Figure S7B), causes embryonic lethality of both homozygotes and trans-heterozygotes with *dsb* deficiencies. The effectiveness of *dsb RNAi* was confirmed by the potent knockdown of Dsb-GFP transgene expression by *UAS-dsb RNAi* designed against the last exon of *dsb* with no predicted off-targets (Figures S7C and S7E), but not by the control *UAS-crq RNAi* (Figures S7D and S7E).

Because larvae expressing Dsb-GFP in the epidermis were sick after 72 hr AEL and showed spontaneous dendrite fragmentation (Figure S7F-S7F"), while pupae with Dsb-GFP expression in the epidermis showed normal dendrite pruning, we focused on examining the distribution of Dsb transgenes in the pupa. Dsb-GFP is localized in intracellular vesicles that

largely coincide with tdTom+ phagosomes even though Dsb-GFP and tdTom are differentially enriched in these phagosomes (Figures 7E-7E"). While only a small portion of Dsb-GFP vesicles overlapped with Rab7+ donut structures (Figures 7F-7F"), Dsb-HA showed more extensive overlap with GFP-LAMP (Figures 7G-7G"), suggesting that Dsb is mainly localized in degradative compartments such as lysosomes and phagolysosomes. As the mammalian CD36 family member with the highest homology to Dsb is the lysosomal membrane protein LIMP-2 (Kuronita et al., 2002), this subcellular localization may reflect an evolutionarily conserved function shared by Dsb and LIMP-2.

The clearance phenotypes caused by *dsb* knockdown are similar to those of Lamp1 RNAi, indicating that Dsb functions downstream of Rab7. Indeed, knockdown of Rab7 in pupal epidermal cells blocked association of Dsb-GFP with tdTom+ phagosomes (Figures 7H-7H"), whereas knocking down *dsb* did not disrupt the association of Rab7-GFP with tdTom+ phagosomes (Figures 7I-7I", compared to Figures 2C-2C"). Since *dsb* RNAi did not prevent the association of GFP-LAMP with tdTom-labeled phagosomes in epidermal cells (Figures 7J-7J", compared to Figures 2D-2D"), Dsb likely acts downstream of, or in parallel with, Lamp1 in the maturation of dendrite-derived phagosomes.

The phagocytic activity of epidermal cells facilitates dendrite fragmentation during degeneration

Besides dendrite clearance defects, we frequently observed delay of dendrite fragmentation when genes involved in engulfment and phagosome maturation were knocked down in the epidermis. We quantified this effect in animals expressing RNAi against Drpr, Vps16A, and WASp. Knockdown of Vps16A, a subunit of the class C Vps complex required for lysosomal delivery (Pulipparacharuvil et al., 2005; Rieder and Emr, 1997), in epidermal cells blocked degradation of CD4-tdGFP on dendrite debris (data not shown). WASp is a regulator of actin polymerization involved in the formation of the phagocytic cup during engulfment (Lorenzi et al., 2000; Zhang et al., 1999) and can be partially knocked down with RNAi expression in epidermal cells (Figures S8A and S8A'). Dendrite fragmentation was delayed in dendrite pruning when these RNAi constructs were expressed in the epidermal sheets so that many abdominal segments contained *ppk-CD4-tdGFP*-labeled dendrites longer than 50 μm at 16 hr APF (Figure 8B-8E), while no such branches were detectable in control animals (Figures 8A and 8E). Knockdown of these genes also led to an increase in the length of unfragmented dendrites at 6 hr AI (Figures 8G-8J) compared to the control (Figure 8F and 8J) in larvae with dendrite injury. By expressing GFP-moesin (GMA) in epidermal cells to label actin filaments (Kiehart et al., 2000) and CD4-tdTom in class IV da neurons to label dendrites during fragmentation, we monitored phagocytic interactions of epidermal cells with dendrites via time-lapse imaging. In control prepupae, low order dendrite branches that showed signs of degeneration such as thinning and beading (Williams and Truman, 2005) were wrapped by dynamic, actin-rich membrane structures of epidermal cells throughout the process of fragmentation (Figure 8K and Movie S6). In contrast, *drpr* RNAi expression in the epidermis caused the lower order dendrite branches to degenerate without being associated by actin-rich epidermal membranes (Figure 8L and Movie S7). These data show that, rather than just internalizing disintegrated dendrite pieces, epidermal

cells wrap degenerating dendrites with actin-rich membrane structures through Drpr-mediated recognition to facilitate dendrite breakdown.

DISCUSSION

Removal of nonfunctional or damaged tissues is an important biological process during tissue remodeling or repair. Here we show that, for *Drosophila* class IV da neurons in the periphery, degenerating dendrites in both dendrite pruning and injury models are removed by neighboring epithelial cells rather than professional phagocytes. By developing multiple dendritic markers that labels phagosomes differentially, we established the clearance of degenerating dendrites as an *in vivo* model to study phagocytosis. With these tools, we analyzed key players in engulfment and phagosome maturation, and elucidated novel roles of the CD36 family members Crq and Dsb. Our study further reveals that, as phagocytes, epidermal cells actively participate in not only the removal but also the fragmentation of degenerating dendrites.

Epidermal cells mediate the clearance of degenerating dendrites

Professional phagocytes such as macrophages in vertebrates and plasmatocytes in *Drosophila* dispose the majority of apoptotic cells in development, as well as invading microorganisms during infection (Meister, 2004; Rabinovitch, 1995). However, non-professional phagocytes may take charge when macrophages or other professional phagocytes are absent or cannot easily access cell corpses, as in apoptosis of rat lens cells (Ishizaki et al., 1993), follicular atresia (Inoue et al., 2000), and degeneration of *Drosophila* egg chambers induced by protein-deprivation (Etchegaray et al., 2012). This scenario does not apply to *Drosophila* da neuronal dendrites, which are exposed to circulating plasmatocytes in the hemolymph and sessile plasmatocytes clustered around da neuron somas (Babcock et al., 2008; Makhijani et al., 2011). Indeed, previous observation of dendrite debris engulfment by plasmatocytes during dendrite pruning has led to the conclusion that plasmatocytes clear pruned dendrites (Williams and Truman, 2005). Our finding that clearance of degenerating dendrites is mainly carried out by epidermal epithelial cells demonstrates that non-professional phagocytes are not just a substitute for professional phagocytes in their absence. Rather, plasmatocytes and epidermal cells likely carry out different functions reflecting specialization of cellular functions. The removal of pruned dendrites by *Drosophila* epidermal cells perhaps can be seen as a parallel to the clearance of photoreceptor outer segments by retinal pigment epithelial cells (Young and Bok, 1969); in both cases epithelial cells maintain homeostasis of the nervous system as part of their physiological functions. The observation that epidermal cells are also responsible for clearing injured dendrites indicates that the same cellular mechanism is also used to cope with perturbations in the peripheral nervous system.

Epithelial cells may profoundly influence the development of dendritic arbors of da neurons. During larval development, growing epithelial cells signal to the dendritic arbors so they can grow proportionally to epithelial cells in order to maintain the same coverage of receptive fields of the sensory neurons, a phenomenon known as dendritic scaling (Parrish et al., 2009). Epithelial cells also contribute to the patterning of dendritic arbors of da neurons by

tethering dendrites to the 2D space of the extracellular matrix so that dendrites have to avoid sister dendrites from the same neuron (self-avoidance) or dendrites from neighboring like-neurons (tiling) (Han et al., 2012; Kim et al., 2012). Our finding that epithelial cells mediate the clearance of degenerating dendrites (this study) substantially adds to the growing list of dendrite properties regulated by epithelial cells.

CD36 family members in engulfment and phagosome maturation

The vertebrate CD36 family members CD36 and scavenger receptor class B type I (SR-BI) mediate phagocytosis of apoptotic cells and microbial pathogens *in vitro* (Krieger, 1999; Silverstein and Febbraio, 2009; Valacchi et al., 2011). The *Drosophila* CD36 family member Crq is required for efficient phagocytosis of cell corpses in embryos (Franc et al., 1999) and mediates binding of apoptotic cells by *in vitro* cultured cells (Franc et al., 1996), leading to its proposed role as a receptor for apoptotic cells. In this study, we show that in epithelial cells *crq* is required for phagosome maturation but not for the engulfment of degenerating dendrites. As loss of *crq* does not completely abolish the engulfment of apoptotic cells in the embryo (Franc et al., 1999), it is possible that the cell-corpse clearance defect in *crq* mutant embryos may be a consequence of blocked phagosome maturation. An alternative possibility is that Crq may be required for engulfment and/or phagosome maturation of apoptotic cells by embryonic macrophages but only required for phagosome maturation of pruned or injured dendrites by epithelial cells. This could be due to the fact that macrophages have to actively search for and bind apoptotic cells, while epithelial cells engulf neighboring debris. Further experiments will be needed to determine whether Crq also plays a role in phagosome maturation during phagocytosis by macrophages.

Loss of Crq function resulted in the fusion of dendrite-derived phagosomes accompanied with a failure of degradation of phagosome contents, most likely due to inefficient delivery of degradation machineries to late phagosomes. As phagosomes normally acquire hydrolases and other phagolysosomal components by fusing with endosomes and lysosomes, we hypothesize that Crq suppresses homotypic phagosome fusion to promote fusion between phagosomes and late endosomes/lysosomes. Homotypic phagosome fusion rarely happens during normal phagocytosis but is induced by infection of bacterial pathogens such as *Helicobacter pylori* and *Chlamydia trachomatis* (Allen et al., 2000; Majeed et al., 1999); the ability of different strains of *H. pylori* to induce phagosome fusion correlates with the virulence and intracellular survival of these bacteria (Allen et al., 2000; Schwartz and Allen, 2006). Therefore, regulation of the balance between homotypic phagosome fusion and heterotypic fusion between phagosomes and late endosomes/lysosomes is likely critical for the degradation of internalized materials.

The *Drosophila* genome encodes fourteen CD36 family members. Besides the involvement of Crq in phagocytosis, another member Pes mediates mycobacteria infection (Philips et al., 2005). In this study, we found that the CD36 family member Dsb regulates late stages of phagosome maturation. Interestingly, LIMP-2, the mammalian CD36 family member with the highest homology to Dsb, is an intrinsic lysosomal protein required for the degradation of *Listeria* in phagosomes (Carrasco-Marin et al., 2011). Dsb and LIMP-2 thus appear to have evolutionarily conserved functions in phagosome maturation.

Phagocytes promote neurite degeneration

Phagocytes not only clear cell corpses but may also engulf still-living cells and promote cellular degeneration in many contexts (Conradt, 2002). In this study we show that efficient degeneration of dendrites requires the coordination with phagocytic epithelial cells. One mechanism for such coordination is the Drpr-mediated recognition of degenerating dendrites by epidermal phagocytes that form actin-rich membrane structures wrapping around the dendrites to facilitate their fragmentation. In the postnatal mouse brain, microglia actively induce apoptosis of Purkinje cells by producing superoxide ions (Marin-Teva et al., 2004). It remains to be determined whether non-professional phagocytes such as epidermal cells also promote neurite degeneration by emitting diffusible agents.

EXPERIMENTAL PROCEDURES

Live Imaging and dendrite lesion

Animals were reared at 25°C in density-controlled vials. Pupae older than 12 hr APF were dissected out of pupal cases and mounted in imaging chambers constructed on regular glass slides. Prepupae (before 12 hr APF) were directly mounted in the imaging chamber. For dendrite lesion, anesthetized larvae at 72 hr AEL mounted on slides were targeted using a 930 nm 2-photon laser at the primary dendrites of ddaC neurons. Animals were recovered on grape juice agar plates following lesion and imaged at appropriate times. All imaging was done using a Leica SP5 microscope. Unless noted otherwise, confocal images shown in all figures are maximum intensity projections of z-stacks encompassing the epidermal layer and the sensory neurons beneath, which are typically 8-10 μm for larvae and 12-15 μm for pupae.

The detailed descriptions for *Drosophila* stocks, molecular cloning, targeting of the *crq* locus, RNAi and Shi^{ts} expression, immunohistochemistry, imaging, TEM, image analysis and quantification can be found in Supplemental Experimental Procedures.

Supplementary Material

Refer to Web version on PubMed Central for supplementary material.

Acknowledgments

We thank Michael Galko, Sergey Sinenko, Katja Brückner, Hugo Bellen, Helmut Krä mer, David Casso, Ulrike Heberlein, Marc Freeman, Estee Kurant, Sougata Roy, Bloomington Stock Center, and VDRC for fly stocks; Akira Nakamura for antibodies; Bree Grillo-Hill and DGRC for plasmids; Michael Grabe, Seymour Packman, Jean Olson, and members of the Jan lab for discussion. This work was supported by a postdoctoral fellowship from the Jane Coffin Childs Memorial Fund to C.H., an Irvington Institute fellowship from the Cancer Research Institute to H.X., a TSRI Advanced Discovery Institute start-up grant provided by Novartis and NIH grant (R01 AI093687-01A1) to N.C.F., and NIH grant (2R37NS040929) to Y.N.J.. L.Y.J. and Y.N.J. are investigators of Howard Hughes Medical Institute. This is manuscript #25084 from The Scripps Research Institute.

REFERENCES

Aldskogius H, Kozlova EN. Central neuron-glial and glial-glial interactions following axon injury. Prog Neurobiol. 1998; 55:1–26. [PubMed: 9602498]

Allen LA, Schlesinger LS, Kang B. Virulent strains of Helicobacter pylori demonstrate delayed phagocytosis and stimulate homotypic phagosome fusion in macrophages. J Exp Med. 2000; 191:115–128. [PubMed: 10620610]

Awasaki T, Ito K. Engulfing action of glial cells is required for programmed axon pruning during Drosophila metamorphosis. Curr Biol. 2004; 14:668–677. [PubMed: 15084281]

Awasaki T, Tatsumi R, Takahashi K, Arai K, Nakanishi Y, Ueda R, Ito K. Essential role of the apoptotic cell engulfment genes draper and ced-6 in programmed axon pruning during Drosophila metamorphosis. Neuron. 2006; 50:855–867. [PubMed: 16772168]

Babcock DT, Brock AR, Fish GS, Wang Y, Perrin L, Krasnow MA, Galko MJ. Circulating blood cells function as a surveillance system for damaged tissue in Drosophila larvae. Proc Natl Acad Sci U S A. 2008; 105:10017–10022. [PubMed: 18632567]

Botelho RJ, Grinstein S. Phagocytosis. Curr Biol. 2011; 21:R533–538.

Braun A, Hoffmann JA, Meister M. Analysis of the Drosophila host defense in domino mutant larvae, which are devoid of hemocytes. Proc Natl Acad Sci U S A. 1998; 95:14337–14342. [PubMed: 9826701]

Carrasco-Marin E, Fernandez-Prieto L, Rodriguez-Del Rio E, Madrazo-Toca F, Reinheckel T, Saftig P, Alvarez-Dominguez C. LIMP-2 links late phagosomal trafficking with the onset of the innate immune response to Listeria monocytogenes: a role in macrophage activation. J Biol Chem. 2011; 286:3332–3341. [PubMed: 21123180]

Conradt B. With a little help from your friends: cells don't die alone. Nat Cell Biol. 2002; 4:E139–143. [PubMed: 12042826]

Cuttell L, Vaughan A, Silva E, Escaron CJ, Lavine M, Van Goethem E, Eid JP, Quirin M, Franc NC. Undertaker, a Drosophila Junctophilin, links Draper-mediated phagocytosis and calcium homeostasis. Cell. 2008; 135:524–534. [PubMed: 18984163]

Doherty J, Logan MA, Tasdemir OE, Freeman MR. Ensheathing glia function as phagocytes in the adult Drosophila brain. J Neurosci. 2009; 29:4768–4781. [PubMed: 19369546]

Dubois L, Lecourtois M, Alexandre C, Hirst E, Vincent JP. Regulated endocytic routing modulates wingless signaling in Drosophila embryos. Cell. 2001; 105:613–624. [PubMed: 11389831]

Etchegaray JI, Timmons AK, Klein AP, Pritchett TL, Welch E, Meehan TL, Li C, McCall K. Draper acts through the JNK pathway to control synchronous engulfment of dying germline cells by follicular epithelial cells. Development. 2012; 139:4029–4039. [PubMed: 22992958]

Franc NC, Dimarcq JL, Lagueux M, Hoffmann J, Ezekowitz RA. Croquemort, a novel Drosophila hemocyte/macrophage receptor that recognizes apoptotic cells. Immunity. 1996; 4:431–443. [PubMed: 8630729]

Franc NC, Heitzler P, Ezekowitz RA, White K. Requirement for croquemort in phagocytosis of apoptotic cells in Drosophila. Science. 1999; 284:1991–1994. [PubMed: 10373118]

Frank-Cannon TC, Alto LT, McAlpine FE, Tansey MG. Does neuroinflammation fan the flame in neurodegenerative diseases? Mol Neurodegener. 2009; 4:47. [PubMed: 19917131]

Fuentes-Medel Y, Logan MA, Ashley J, Ataman B, Budnik V, Freeman MR. Glia and muscle sculpt neuromuscular arbors by engulfing destabilized synaptic boutons and shed presynaptic debris. PLoS Biol. 2009; 7:e1000184. [PubMed: 19707574]

Gong WJ, Golic KG. Ends-out, or replacement, gene targeting in Drosophila. Proc Natl Acad Sci U S A. 2003; 100:2556–2561. [PubMed: 12589026]

Hall S. The response to injury in the peripheral nervous system. J Bone Joint Surg Br. 2005; 87:1309–1319. [PubMed: 16189300]

Han C, Jan LY, Jan YN. Enhancer-driven membrane markers for analysis of nonautonomous mechanisms reveal neuron-glia interactions in Drosophila. Proc Natl Acad Sci U S A. 2011; 108:9673–9678. [PubMed: 21606367]

Han C, Wang D, Soba P, Zhu S, Lin X, Jan LY, Jan YN. Integrins regulate repulsion-mediated dendritic patterning of drosophila sensory neurons by restricting dendrites in a 2D space. Neuron. 2012; 73:64–78. [PubMed: 22243747]

Huynh KK, Eskelinen EL, Scott CC, Malevanets A, Saftig P, Grinstein S. LAMP proteins are required for fusion of lysosomes with phagosomes. EMBO J. 2007; 26:313–324. [PubMed: 17245426]

Inoue S, Watanabe H, Saito H, Hiroi M, Tonosaki A. Elimination of atretic follicles from the mouse ovary: a TEM and immunohistochemical study in mice. J Anat. 2000; 196(Pt 1):103–110. [PubMed: 10697292]

Ishizaki Y, Voyvodic JT, Burne JF, Raff MC. Control of lens epithelial cell survival. J Cell Biol. 1993; 121:899–908. [PubMed: 8491781]

Katayama H, Yamamoto A, Mizushima N, Yoshimori T, Miyawaki A. GFP-like proteins stably accumulate in lysosomes. Cell Struct Funct. 2008; 33:1–12. [PubMed: 18256512]

Kiehart DP, Galbraith CG, Edwards KA, Rickoll WL, Montague RA. Multiple forces contribute to cell sheet morphogenesis for dorsal closure in Drosophila. J Cell Biol. 2000; 149:471–490. [PubMed: 10769037]

Kim ME, Shrestha BR, Blazeski R, Mason CA, Grueber WB. Integrins establish dendrite-substrate relationships that promote dendritic self-avoidance and patterning in drosophila sensory neurons. Neuron. 2012; 73:79–91. [PubMed: 22243748]

Kinchen JM, Ravichandran KS. Phagosome maturation: going through the acid test. Nat Rev Mol Cell Biol. 2008; 9:781–795. [PubMed: 18813294]

Krieger M. Charting the fate of the “good cholesterol”: identification and characterization of the high-density lipoprotein receptor SR-BI. Annu Rev Biochem. 1999; 68:523–558. [PubMed: 10872459]

Kuo CT, Jan LY, Jan YN. Dendrite-specific remodeling of Drosophila sensory neurons requires matrix metalloproteases, ubiquitin-proteasome, and ecdysone signaling. Proc Natl Acad Sci U S A. 2005; 102:15230–15235. [PubMed: 16210248]

Kurant E, Axelrod S, Leaman D, Gaul U. Six-microns-under acts upstream of Draper in the glial phagocytosis of apoptotic neurons. Cell. 2008; 133:498–509. [PubMed: 18455990]

Kuronita T, Eskelinen EL, Fujita H, Saftig P, Himeno M, Tanaka Y. A role for the lysosomal membrane protein LGP85 in the biogenesis and maintenance of endosomal and lysosomal morphology. J Cell Sci. 2002; 115:4117–4131. [PubMed: 12356916]

Lee HH, Jan LY, Jan YN. Drosophila IKK-related kinase Ik2 and Katanin p60-like 1 regulate dendrite pruning of sensory neuron during metamorphosis. Proc Natl Acad Sci U S A. 2009; 106:6363–6368. [PubMed: 19329489]

Li W, Baker NE. Engulfment is required for cell competition. Cell. 2007; 129:1215–1225. [PubMed: 17574031]

Lorenzi R, Brickell PM, Katz DR, Kinnon C, Thrasher AJ. Wiskott-Aldrich syndrome protein is necessary for efficient IgG-mediated phagocytosis. Blood. 2000; 95:2943–2946. [PubMed: 10779443]

Luo L, O'Leary DD. Axon retraction and degeneration in development and disease. Annu Rev Neurosci. 2005; 28:127–156. [PubMed: 16022592]

MacDonald JM, Beach MG, Porpiglia E, Sheehan AE, Watts RJ, Freeman MR. The Drosophila cell corpse engulfment receptor Draper mediates glial clearance of severed axons. Neuron. 2006; 50:869–881. [PubMed: 16772169]

Majeed M, Krause KH, Clark RA, Kihlstrom E, Stendahl O. Localization of intracellular Ca2+ stores in HeLa cells during infection with Chlamydia trachomatis. J Cell Sci. 1999; 112(Pt 1):35–44. [PubMed: 9841902]

Makhijani K, Alexander B, Tanaka T, Rulifson E, Bruckner K. The peripheral nervous system supports blood cell homing and survival in the Drosophila larva. Development. 2011; 138:5379–5391. [PubMed: 22071105]

Marin-Teva JL, Dusart I, Colin C, Gervais A, van Rooijen N, Mallat M. Microglia promote the death of developing Purkinje cells. Neuron. 2004; 41:535–547. [PubMed: 14980203]

Meister M. Blood cells of Drosophila: cell lineages and role in host defence. Curr Opin Immunol. 2004; 16:10–15. [PubMed: 14734104]

Miesenbock G, De Angelis DA, Rothman JE. Visualizing secretion and synaptic transmission with pH-sensitive green fluorescent proteins. Nature. 1998; 394:192–195. [PubMed: 9671304]

Nichols Z, Vogt RG. The SNMP/CD36 gene family in Diptera, Hymenoptera and Coleoptera: Drosophila melanogaster, D. pseudoobscura, Anopheles gambiae, Aedes aegypti, Apis mellifera, and Tribolium castaneum. Insect Biochem Mol Biol. 2008; 38:398–415. [PubMed: 18342246]

Parrish JZ, Xu P, Kim CC, Jan LY, Jan YN. The microRNA bantam functions in epithelial cells to regulate scaling growth of dendrite arbors in drosophila sensory neurons. Neuron. 2009; 63:788–802. [PubMed: 19778508]

Philips JA, Rubin EJ, Perrimon N. Drosophila RNAi screen reveals CD36 family member required for mycobacterial infection. Science. 2005; 309:1251–1253. [PubMed: 16020694]

Pulipparacharuvil S, Akbar MA, Ray S, Sevrioukov EA, Haberman AS, Rohrer J, Kramer H. Drosophila Vps16A is required for trafficking to lysosomes and biogenesis of pigment granules. J Cell Sci. 2005; 118:3663–3673. [PubMed: 16046475]

Rabinovitch M. Professional and non-professional phagocytes: an introduction. Trends Cell Biol. 1995; 5:85–87. [PubMed: 14732160]

Rieder SE, Emr SD. A novel RING finger protein complex essential for a late step in protein transport to the yeast vacuole. Mol Biol Cell. 1997; 8:2307–2327. [PubMed: 9362071]

Savill J, Hogg N, Ren Y, Haslett C. Thrombospondin cooperates with CD36 and the vitronectin receptor in macrophage recognition of neutrophils undergoing apoptosis. J Clin Invest. 1992; 90:1513–1522. [PubMed: 1383273]

Saxena S, Caroni P. Mechanisms of axon degeneration: from development to disease. Prog Neurobiol. 2007; 83:174–191. [PubMed: 17822833]

Schwartz JT, Allen LA. Role of urease in megasome formation and Helicobacter pylori survival in macrophages. J Leukoc Biol. 2006; 79:1214–1225. [PubMed: 16543403]

Silverstein RL, Febbraio M. CD36, a scavenger receptor involved in immunity, metabolism, angiogenesis, and behavior. Sci Signal. 2009; 2:re3. [PubMed: 19471024]

Song JW, Misgeld T, Kang H, Knecht S, Lu J, Cao Y, Cotman SL, Bishop DL, Lichtman JW. Lysosomal activity associated with developmental axon pruning. J Neurosci. 2008; 28:8993–9001. [PubMed: 18768693]

Song Y, Ori-McKenney KM, Zheng Y, Han C, Jan LY, Jan YN. Regeneration of Drosophila sensory neuron axons and dendrites is regulated by the Akt pathway involving Pten and microRNA bantam. Genes Dev. 2012; 26:1612–1625. [PubMed: 22759636]

Stuart LM, Deng J, Silver JM, Takahashi K, Tseng AA, Hennessy EJ, Ezekowitz RA, Moore KJ. Response to Staphylococcus aureus requires CD36-mediated phagocytosis triggered by the COOH-terminal cytoplasmic domain. J Cell Biol. 2005; 170:477–485. [PubMed: 16061696]

Stuart LM, Ezekowitz RA. Phagocytosis and comparative innate immunity: learning on the fly. Nat Rev Immunol. 2008; 8:131–141. [PubMed: 18219310]

Tao J, Rolls MM. Dendrites have a rapid program of injury-induced degeneration that is molecularly distinct from developmental pruning. J Neurosci. 2011; 31:5398–5405. [PubMed: 21471375]

Tepass U, Fessler LI, Aziz A, Hartenstein V. Embryonic origin of hemocytes and their relationship to cell death in Drosophila. Development. 1994; 120:1829–1837. [PubMed: 7924990]

Valacchi G, Sticozzi C, Lim Y, Pecorelli A. Scavenger receptor class B type I: a multifunctional receptor. Ann N Y Acad Sci. 2011; 1229:E1–7. [PubMed: 22239457]

Verkhusha VV, Kuznetsova IM, Stepanenko OV, Zaraisky AG, Shavlovsky MM, Turoverov KK, Uversky VN. High stability of Discosoma DsRed as compared to Aequorea EGFP. Biochemistry. 2003; 42:7879–7884. [PubMed: 12834339]

Watts RJ, Schuldiner O, Perrino J, Larsen C, Luo L. Glia engulf degenerating axons during developmental axon pruning. Curr Biol. 2004; 14:678–684. [PubMed: 15084282]

Williams DW, Kondo S, Krzyzanowska A, Hiromi Y, Truman JW. Local caspase activity directs engulfment of dendrites during pruning. Nat Neurosci. 2006; 9:1234–1236. [PubMed: 16980964]

Williams DW, Truman JW. Cellular mechanisms of dendrite pruning in Drosophila: insights from in vivo time-lapse of remodeling dendritic arborizing sensory neurons. Development. 2005; 132:3631–3642. [PubMed: 16033801]

Wood W, Turmaine M, Weber R, Camp V, Maki RA, McKercher SR, Martin P. Mesenchymal cells engulf and clear apoptotic footplate cells in macrophageless PU.1 null mouse embryos. Development. 2000; 127:5245–5252. [PubMed: 11076747]

Wucherpfennig T, Wilsch-Brauninger M, Gonzalez-Gaitan M. Role of Drosophila Rab5 during endosomal trafficking at the synapse and evoked neurotransmitter release. J Cell Biol. 2003; 161:609–624. [PubMed: 12743108]

Young RW, Bok D. Participation of the retinal pigment epithelium in the rod outer segment renewal process. J Cell Biol. 1969; 42:392–403. [PubMed: 5792328]

Yu X, Odera S, Chuang CH, Lu N, Zhou Z. C. elegans Dynamin mediates the signaling of phagocytic receptor CED-1 for the engulfment and degradation of apoptotic cells. Dev Cell. 2006; 10:743–757. [PubMed: 16740477]

Zhang J, Shehabeldin A, da Cruz LA, Butler J, Somani AK, McGavin M, Kozieradzki I, dos Santos AO, Nagy A, Grinstein S, et al. Antigen receptor-induced activation and cytoskeletal rearrangement are impaired in Wiskott-Aldrich syndrome protein-deficient lymphocytes. J Exp Med. 1999; 190:1329–1342. [PubMed: 10544204]

Zhou Z, Hartwieg E, Horvitz HR. CED-1 is a transmembrane receptor that mediates cell corpse engulfment in C. elegans. Cell. 2001; 104:43–56. [PubMed: 11163239]

Zhou Z, Yu X. Phagosome maturation during the removal of apoptotic cells: receptors lead the way. Trends Cell Biol. 2008; 18:474–485. [PubMed: 18774293]

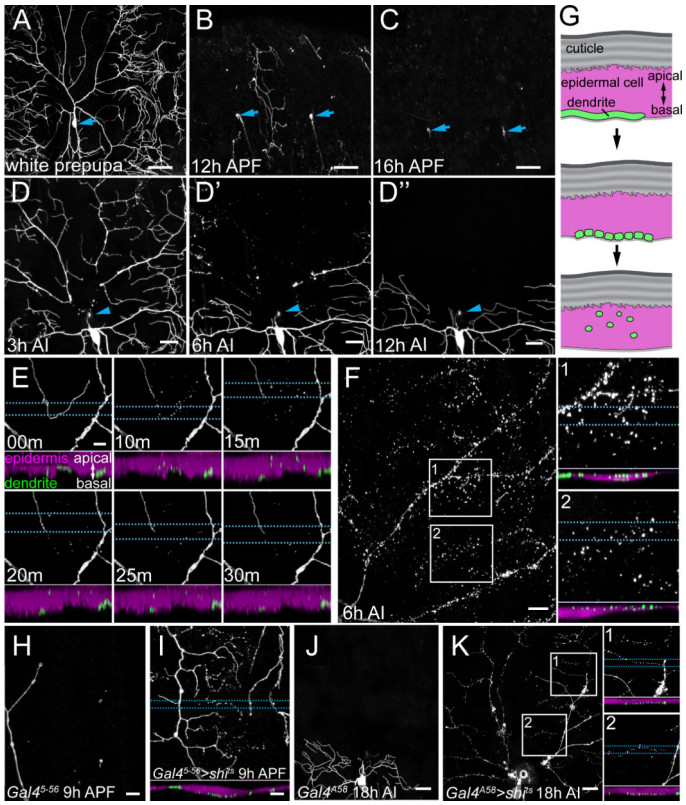

Figure 1. Epidermal epithelia clear dendrite debris during dendrite pruning and after dendrite injury

(A-D") Time course of dendrite degeneration of class IV da neurons labeled by *ppk-CD4-tdGFP* during dendrite pruning (A-C) and after dendrite injury (D-D"). The cell bodies are indicated by arrows in (A-C) and the sites of injury are indicated by arrowheads in (D-D"). (E) Time-lapse images of a terminal dendrite undergoing fragmentation during pruning. The upper panels show Z-axis projections. The bottom panels are Y-axis projections of the volumes encompassed between the two dotted lines showing the relative position of dendrites and dendrite debris labeled by CD4-tdGFP (green) and epidermal cells labeled by tdTom (magenta) along the apical-basal axis. (F) Dendrites undergoing degeneration at 6 hr after injury (AI). The enlarged views of the boxed regions are shown in the panels on the right. (G) A diagram illustrating cross sections of the body wall and the dislocation of dendrite debris into the epidermal cell layer after dendrite fragmentation. (H and I) Dendrite debris labeled by CD4-tdGFP in *Gal4*$^{5\text{-}56}$>*mCherry* control (H) and *Gal4*$^{5\text{-}56}$>*shi*^{ts}, *mCherry* (I) incubated at 29°C from 3-9 hr after puparium formation (APF). (J and K) Dendrite debris labeled by CD4-tdGFP in *Gal4*^{A58}>*tdTom* control (J) and *Gal4*^{A58}>*shi*^{ts}, *tdTom* (K) incubated at 29°C from 0-18 hr AI. The details of the boxed regions in (K) are shown in the panels on the right. Scale bars: 50 μm in (A-C); 20 μm in (D-D", J, and K); 5 μm in (E, F', and F"); 10 μm in (F, H, and I). See also Figure S1 and Movie S1.

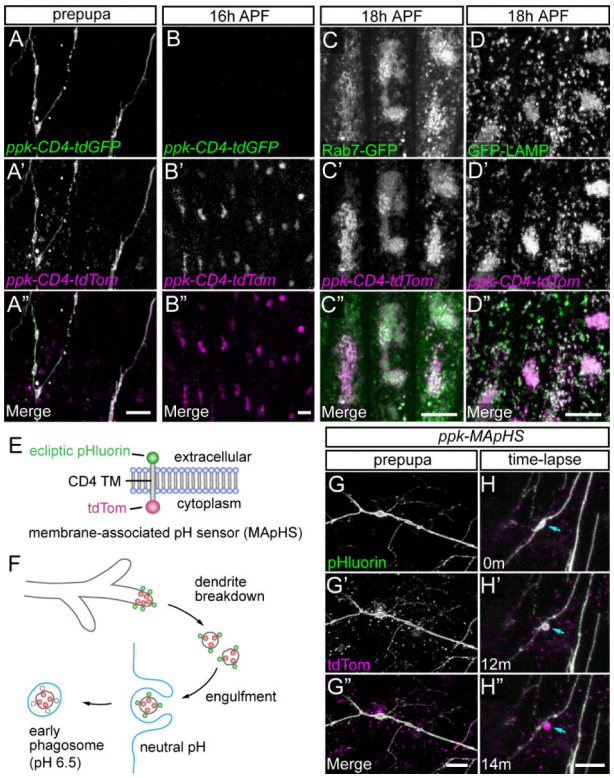

Figure 2. Dendritic markers for analyzing engulfment of dendrite debris and phagolysosome maturation

(A-B") Comparison of CD4-tdGFP and CD4-tdTom in labeling dendrite-derived phagosomes during dendrite pruning. (C-D") Colocalization of dendrite-derived tdTom with Rab7-GFP (C-C") and GFP-LAMP (D-D") at 18 hr APF. (E) Diagram of the domain structure and topology of the MApHS marker. CD4 TM: CD4 transmembrane domain. (F) Diagram of using MApHS to monitor the initial acidification of dendrite-derived phagosomes. (G-G") Labeling of dendrite debris by MApHS during dendrite pruning. (H-H") Time-lapse images of MApHS-labeled degenerating dendrites showing quenching of pHluorin in a newly formed shedosome (arrow). In all merged panels, GFP and pHluorin signals are in green and tdTom signals are in magenta. Scale bars represent 10 μm in all panels. See also Figure S2 and Movies S2 and S3.

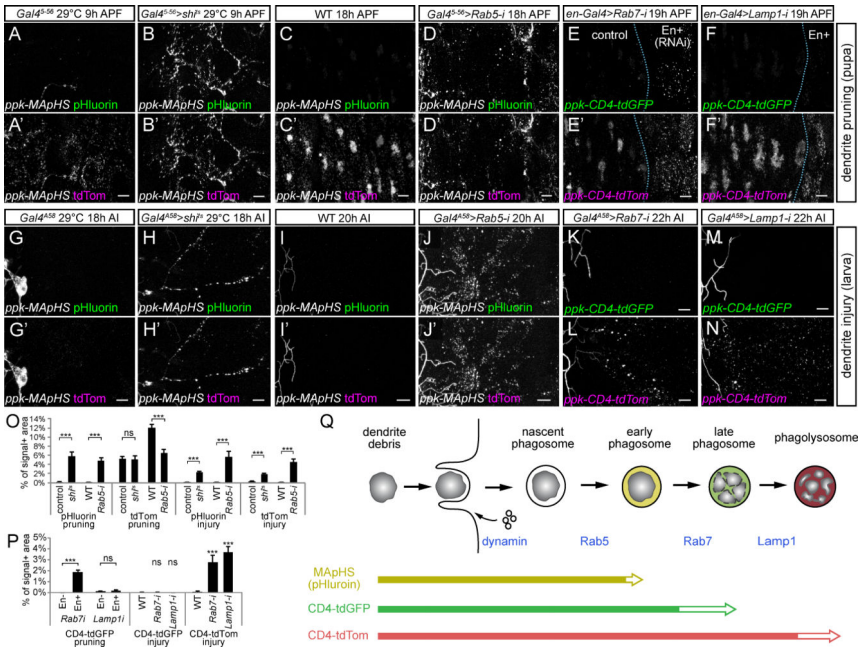

Figure 3. Dissecting phagocytosis of dendrite debris with dendritic markers

(A-B') Clearance of pruned dendrites in *Gal4*$^{5\text{-}56}$ control (A and A') and *Gal4*$^{5\text{-}56}$>*shi*^{ts} (B and B') at 29°C during 3-9 hr APF. (C-F') Clearance of pruned dendrites in the wildtype (WT) (C and C') and animals with epidermis-specific knockdown of *Rab5* (*Rab5-i*) (D and D'), *Rab7* (*Rab7-i*) (E and E'), and *Lamp1* (*Lamp1-i*) (F and F') in pupae. The expression of UAS-RNAi was driven by *Gal4*$^{5\text{-}56}$ (D and D'), or by *en-Gal4* (E-F') in the posterior half of each abdominal segment (En+), thus the anterior half (En-) serves as an internal control. The boundaries between En+ cells and En- cells are marked by dotted lines. (G-H') Clearance of injured dendrites in *Gal4*^{A58} control (G and G') and *Gal4*^{A58}>*shi*^{ts} (H and H') at 29°C during 0-18 hr AI. (I-N) Clearance of injured dendrites in WT (I and I') and animals with *Gal4*^{A58}-driven epidermis-specific knockdown of *Rab5* (J and J'), *Rab7* (K and L), and *Lamp1* (M and N) in larvae. Scale bars =10 μm. (O) Quantification of dendrite clearance phenotypes in *shi*^{ts} overexpression and *Rab5* knockdown in both dendrite pruning and dendrite injury models. The retention of pHluorin and tdTom signals is reflected by the percentage of signal+ pixels (% of signal+ area). (P) Quantification of dendrite clearance phenotypes in the knockdown of *Rab7* and *Lamp1* in both dendrite pruning and dendrite injury, showing percentages of tdGFP+ and tdTom+ areas. TdTom was not quantified for dendrite pruning as it also persisted in the WT. For dendrite pruning, En- areas were used as controls. Error bars = SEM. ***p < 0.001; ns, not significant; oneway analysis of variance and Dunnett's test for *Rab7-i* and *Lamp1-i* in dendrite injury and Student's t test for the rest. (Q) Diagram showing the stages at which the labeled genes are required for dendrite clearance and the labeling of phagosomal compartments by the dendritic markers in both larval (solid bars) and pupal (open bars) epidermis. See also Figure S3.

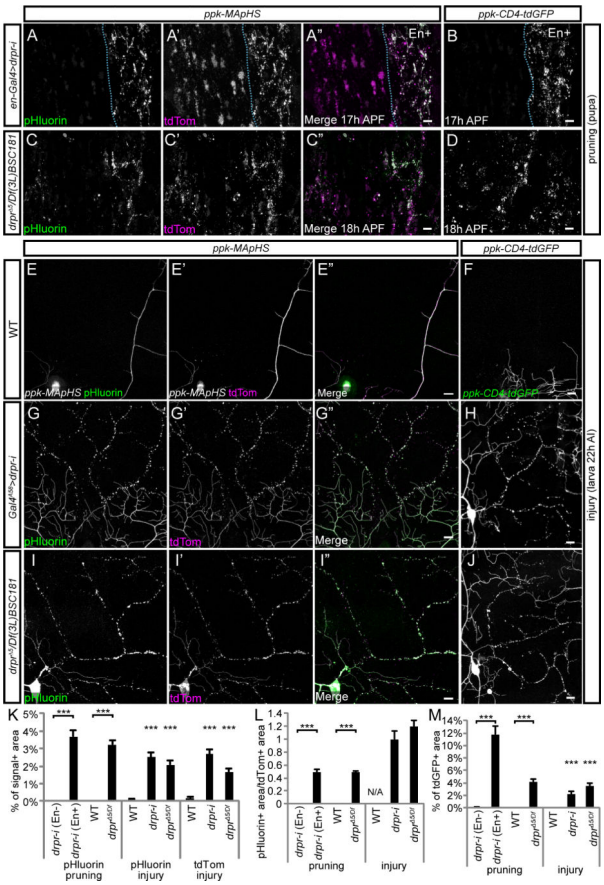

Figure 4. *drpr* is required for engulfment of dendrite debris by epidermal cells

(A-B) Dendrite clearance defects during dendrite pruning in pupae expressing *drpr RNAi* driven by *en-Gal4*. (C-D) Clearance of pruned dendrites in $drpr^{\Delta 5}/Df(3L)BSC181$ mutant pupae. (E-J) Dendrite clearance in the dendrite injury model in WT larvae (E-F), larvae expressing *drpr RNAi* driven by $Gal4^{A58}$ (G-H), and $drpr^{\Delta 5}/Df(3L)BSC181$ mutant larvae (I-J). The dendritic markers and stages of animals are labeled. In merged panels, GFP and pHluorin signals are in green and tdTom signals are in magenta. Scale bars = 10 μm. (K) Quantification of pHluorin and tdTom signals in *drpr* knockdown and mutant. (L) Ratios of pHluorin+ areas over tdTom+ areas in *drpr* knockdown and mutant, reflecting the extent of pHluorin quenching. This ratio was not calculated for WT as tdTom was not retained in WT (N/A, not applicable). (M) Quantification of tdGFP signals in *drpr* knockdown and mutant. Error bars = SEM. ***p < 0.001; ns, not significant; Student's t test for dendrite pruning and oneway analysis of variance and Dunnett's test for dendrite injury. See also Figures S4.

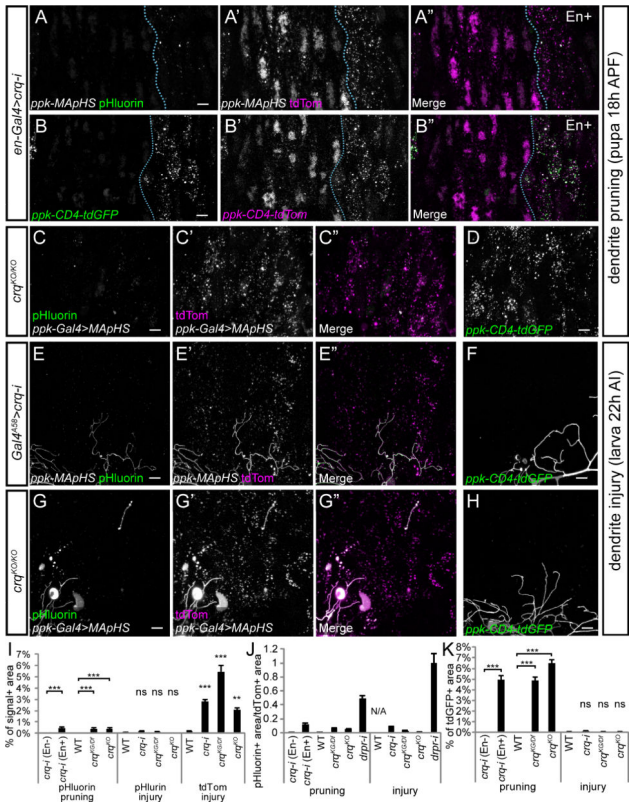

Figure 5. Crq is required for phagosome maturation during the clearance of dendrite debris

(A-B") Dendrite clearance defects during dendrite pruning in *crq* knockdown. (C-D) Dendrite clearance defects during dendrite pruning in homozygous germline-derived crq^{KO} mutant pupae. (E-F) Dendrite clearance defects in the dendrite injury model caused by $Gal4^{A58}$-driven *crq* knockdown. (G-H) Dendrite clearance defects in the dendrite injury model of homozygous germline-derived crq^{KO} mutant larvae. In merged panels, GFP and pHluorin signals are in green and tdTom signals are in magenta. Scale bars =10 μm. (I) Quantification of pHluorin and tdTom signals in *crq* knockdown and mutants. (J) Ratios of pHluorin+ areas over tdTom+ areas in *crq* knockdown and mutants with *drpr* knockdown shown as a comparison. N/A, not applicable. (K) Quantification of tdGFP signals in *crq* knockdown and mutants. Error bars = SEM. **p<0.01, ***p < 0.001; ns, not significant; Student's t test for dendrite pruning and oneway analysis of variance and Dunnett's test for dendrite injury. See also Figures S5.

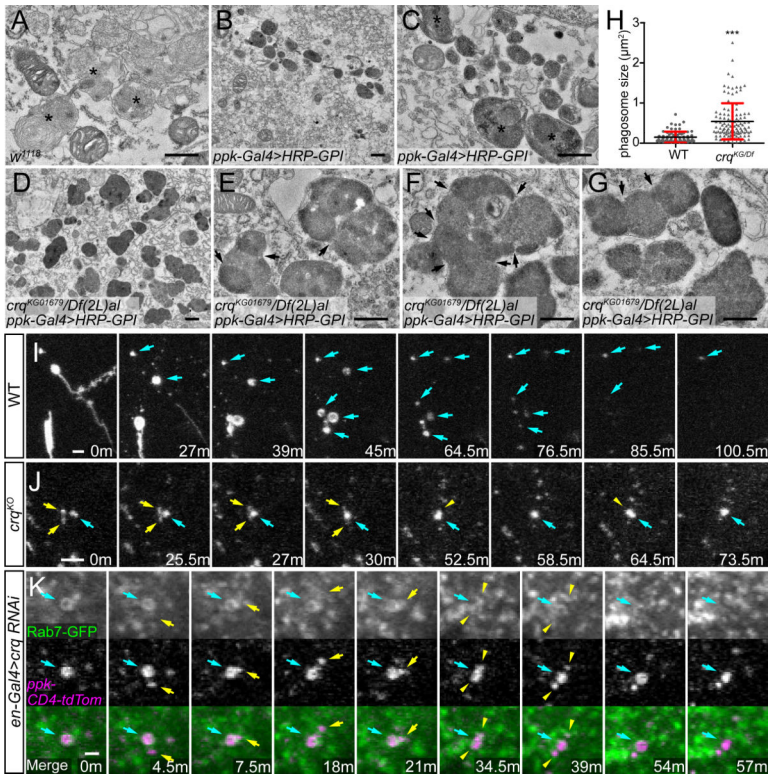

Figure 6. Loss of *crq* leads to homotypic fusion among dendrite-derived phagosomes

(A) TEM image of lysosomes/phagolysosomes in a w^{1118} pupal epidermal cell at 16 hr APF. (B-G) TEM images of dendrite debris-derived phagosomes in epidermal cells of *ppk-Gal4>HRP-GPI* (B and C) and $crq^{KG01679}/Df(2L)al$, *ppk-Gal4>HRP-GPI* (C-F) pupae at 16 hr APF. Dendrite-derived phagosomes are distinguished by intra-phagosomal DAB staining. (B) and (D) are low mag views and (C) and (E-G) are high mag views. The asterisks mark the compartments that are of the typical phagolysosome morphology (A and C). Arrows point to apparent boundaries between individual phagosomes within giant phagosomes in *crq* mutant animals (E-G). (H) Size distribution of DAB+ phagosomes in *ppk-Gal4>HRP-GPI* (WT) and $crq^{KG01679}/Df(2L)al$, *ppk-Gal4>HRP-GPI* ($crq^{KG/Df}$) based on their areas in TEM sections. Black bars represent the mean and red bars represent SD. ***p < 0.001; Student's t test. (I) Time-lapse images showing degradation of CD4-tdGFP-labeled dendrite debris in WT. Arrows point to the dendrite remnants that gradually reduce sizes and lose GFP signals. (J) Time-lapse images showing the persistence of GFP and fusion of GFP+ phagosomes in crq^{KO}. Blue arrows point to a bigger phagosome that fuses with two smaller phagosomes (yellow arrows). Yellow arrowheads indicate the shape change of the phagosome during imaging. The images in (I) and (J) are projections of 9 continuous optical sections covering 9 μm thickness. (K) Time-lapse images showing the dynamics of CD4-tdTom-labeled phagosomes in epidermal cells expressing *crq* RNAi and Rab7-GFP. Blue arrows point to a Rab7-GFP+ phagosome that sequentially fused with two smaller phagosomes (yellow arrows). Yellow arrowheads indicate the shape change and subsequent fission of the phagosome. Rab7-GFP had been released from the phagosome in the last frame. Each panel shows a single optical section to avoid stacking of Rab7-GFP+ vesicles. Phagosome fusion and fission events in (J) and (K) were confirmed in 3D views with the Imaris software. Scale bars: 500 nm in (A-G); 5 μm in (I) and (J); 2 μm in (K). See also Figure S6 and Movies S4 and S5.

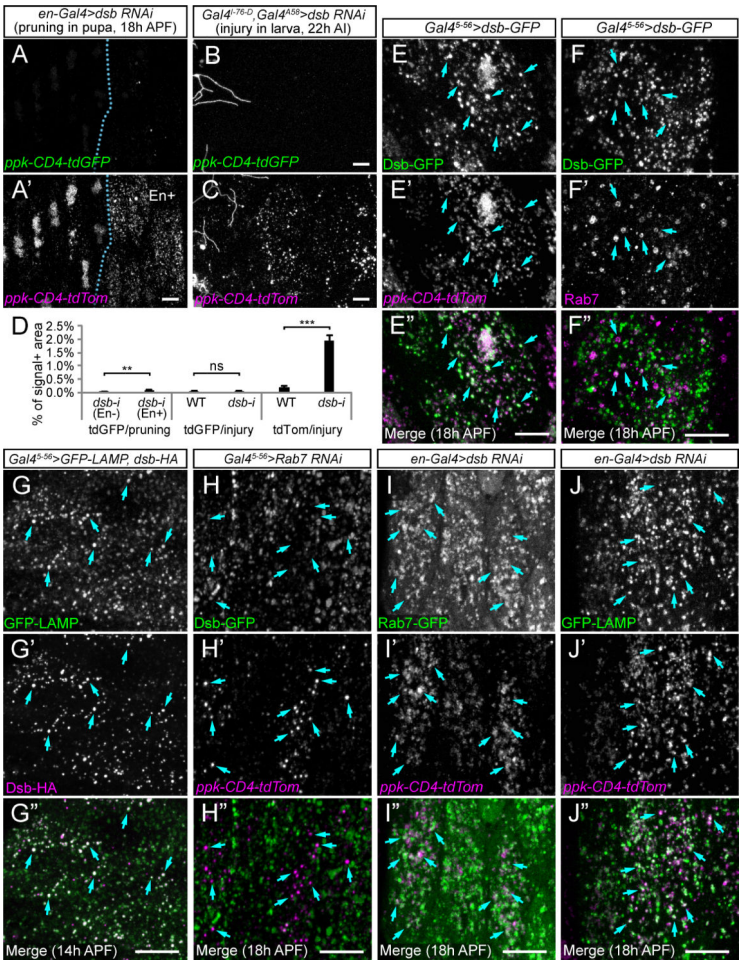

Figure 7. *dsb* encodes a lysosome/phagolysosome protein required for phagosome maturation during the degradation of dendrite debris

(A-A') Clearance of pruned dendrites in *dsb* knockdown driven by *en-Gal4*. (B and C) Clearance of injured dendrites by epidermal cells expressing *dsb* RNAi driven by $Gal4^{I\text{-}76\text{-}D}$, $Gal4^{A58}$. $Gal4^{I\text{-}76\text{-}D}$ is expressed in epidermal cells at embryonic and early larval stages and enhances the *dsb* knockdown phenotype. (D) Quantification of tdGFP and tdTom in *dsb* knockdown in both dendrite pruning and dendrite injury models. Retention of tdTom in dendrite pruning is not shown. Error bars = SEM. **p<0.01, ***p < 0.001; ns, not significant; Student's t test. (E-E") Colocalization of Dsb-GFP with tdTom in phagosomes derived from pruned dendrites at 18 hr APF, shown as projections of 4 continuous optical sections covering 2 μm thickness. (F-F") Partial colocalization of Dsb-GFP with Rab7 in pupal epidermal cells at 18 hr APF, shown as projections of 19 continuous optical sections covering 5.5 μm thickness. (G-G") Extensive colocalization of Dsb-HA with GFP-LAMP in pupal epidermal cells at 14 hr APF, shown as projections of 10 continuous optical sections covering 3 μm thickness. (H-H") Epidermal cells expressing *Rab7* RNAi driven by $Gal4^{5\text{-}56}$ at 18 hr APF showing the lack of colocalization between Dsb-GFP and CD4-tdTom in dendrite-derived phagosomes. Images shown are projections of 9 continuous optical sections covering 3.5 μm thickness. (I-J") Epidermal cells expressing *dsb* RNAi driven *by en-Gal4* at 18 hr APF showing substantial colocalization of Rab7-GFP (I-I") and GFP-LAMP (J-J") with CD4-tdTom in phagosomes. Images shown are projections of 3 continuous optical sections covering 1.3 μm thickness in (I-I") and 5 continuous optical sections covering 2.5 μm thickness in (J-J"). Arrows in (E)-(J") point to a few representative vesicles. Scale bars = 10 μm. See also Figure S7.

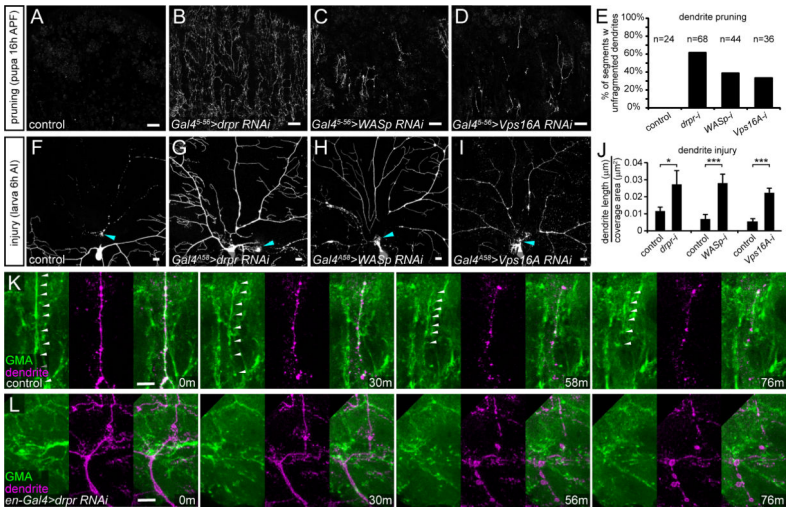

Figure 8. The phagocytic activity of epidermal cells facilitates dendrite fragmentation during dendrite pruning and after dendrite injury

(A-D) Degeneration of CD4-tdGFP-labeled dendrites at 16 hr APF in WT (A) and animals expressing RNAi constructs against *drpr* (B), *WASp* (C), and *Vps16A* (D) in pupal epidermal cells driven by $Gal4^{5\text{-}56}$. (E) Quantification of abdominal segments showing >50 μm dendrites in the WT control and animals expressing *drpr*, *WASp*, *Vps16A* RNAi. (F-I) Degeneration of CD4-tdGFP-labeled dendrites at 6 hr AI in WT (F) and larvae expressing RNAi against *drpr* (G), *WASp* (H), and *Vps16A* (I) in epidermal cells driven by $Gal4^{A58}$. Sites of injury are indicated by arrowheads. (J) Quantification of dendrites in animals expressing *drpr*, *WASp*, *Vps16A* RNAi and their corresponding controls at 6 hr AI. The controls are UAS-RNAi without the $Gal4^{A58}$ driver. Error bars = SEM. *p < 0.05, ***p < 0.001; Student's t test. (K-L) Time-lapse images showing fragmentation of low-order dendrite branches labeled by CD4-tdTom and dynamics of epidermal actin filaments labeled by GMA in an *en-Gal4* control pupa (K) and a pupa expressing *en-Gal4>drpr RNAi* (L). Images shown are projections of 8 continuous optical sections covering 6.4 μm thick tissues and are representative of 16 and 32 time-lapse series for the control and *drpr* knockdown, respectively. Actin-rich epidermal membranes surrounding degenerating dendrites in the control pupa are indicated by arrowheads. Scale bars: 50 μm in (A-D); 10 μm in (F-I); 10 μm in (K) and (L). See also Movies S6 and S7.